

# Horizontal transfer between loose compartments stabilizes replication of fragmented ribozymes

Atsushi Kamimura<sup>1\*</sup>, Yoshiya J. Matsubara<sup>1</sup>, Kunihiko Kaneko<sup>1,2\*</sup>, Nobuto Takeuchi<sup>2,3\*</sup>

**1** Department of Basic Science, Graduate School of Arts and Sciences, The University of Tokyo, 3-8-1, Komaba, Meguro-ku, Tokyo 153-8902 Japan

**2** Research Center for Complex Systems Biology, Graduate School of Arts and Sciences, The University of Tokyo, 3-8-1, Komaba, Meguro-ku, Tokyo 153-8902 Japan

**3** School of Biological Sciences, The University of Auckland, Private Bag 92019, Auckland 1142, New Zealand

\* kamimura@complex.c.u-tokyo.ac.jp(AK), kaneko@complex.c.u-tokyo.ac.jp(KK), nobuto.takeuchi@auckland.ac.nz(NT)

## Abstract

The emergence of replicases that can replicate themselves is a central issue in the origin of life. Recent experiments suggest that such replicases can be realized if an RNA polymerase ribozyme is divided into fragments short enough to be replicable by the ribozyme and if these fragments self-assemble into a functional ribozyme. However, the continued self-replication of such replicases requires that the production of every essential fragment be balanced and sustained. Here, we use mathematical modeling to investigate whether and under what conditions fragmented replicases achieve continued self-replication. We first show that under a simple batch condition, the replicases fail to display continued self-replication owing to positive feedback inherent in these replicases. This positive feedback inevitably biases replication toward a subset of fragments, so that the replicases eventually fail to sustain the production of all essential fragments. We then show that this inherent instability can be resolved by small rates of random content exchange between loose compartments (i.e., horizontal transfer). In this case, the balanced production of all fragments is achieved through negative frequency-dependent selection operating in the population dynamics of compartments. This selection mechanism arises from an interaction mediated by horizontal transfer between intracellular and intercellular symmetry breaking. The horizontal transfer also ensures the presence of all essential fragments in each compartment, sustaining self-replication. Taken together, our results underline compartmentalization and horizontal transfer in the origin of the first self-replicating replicases.

## Author summary

How evolution got started is a crucial question in the origin of life. One possibility is that RNA molecules gained the ability to catalyze self-replication. Researchers recently proposed how this possibility might have been realized: a long RNA catalyst was divided into short replicable fragments, and these fragments self-assembled into the original long catalyst. Ingenious though it is, we expose a hidden flaw in this proposal.

An auto-catalytic system based on fragmented catalysts involves positive feedback, which necessarily biases replication toward specific fragments and eventually halts the replication of the whole system. However, we also propose an effective remedy to this flaw: compartmentalization and content exchange among compartments generate negative feedback, which tightly coordinates the replication of different fragments.

## Introduction

One of the crucial questions in the origin of life is how molecules acquired the capability of undergoing open-ended Darwinian evolution [1, 2]. A potential answer is offered by the template-directed self-replication of a replicase, a replicase that can replicate itself. To determine whether such self-replication is demonstrable in RNA, considerable effort has been devoted to the artificial evolution of RNA polymerase ribozymes [3–10]. A recent milestone in this effort is the demonstration of ‘riboPCR,’ the exponential amplification of RNA through a PCR-like mechanism catalyzed entirely by RNA [8]. The glaring issue, however, has been that the replicases synthesized so far have limitations in processivity and fidelity, so that they can replicate only oligomers much shorter than themselves (or long unstructured cytidine-rich polymers, which exclude the ribozymes themselves).

As a potential solution to this problem, Mutschler et al. and Horning et al. have recently proposed the fragmentation and self-assembly of a replicase. According to their proposals, a replicase is fragmented into multiple sequences that are short enough to be replicable by the replicase and, moreover, capable of self-assembling into a functional replicase [7, 9]. The possibility of reconstituting a functional ribozyme from its fragments through self-assembly has been experimentally demonstrated [7, 9, 10], attesting the chemical plausibility of the proposals.

However, the exponential amplification of multiple distinct fragments raises a question about the dynamical stability of the proposed autocatalytic system. The continued replication of fragmented replicases requires the sustained production of all its essential fragments in yields proportional to the stoichiometric ratio of the fragments in a replicase [11–13]. However, each fragment is replicated by the replicase and thus grows exponentially. If some fragments was replicated persistently faster than the others, the former would out-compete the latter, causing a loss of some essential fragments and hence the cessation of self-replication

The above consideration led us to examine whether and under what conditions fragmented replicases achieve continued self-replication. Using mathematical modeling, we discovered that the fragmented replicases fail to display continued self-replication under a simple batch condition. Replication is inevitably biased toward a subset of the fragments owing to positive feedback inherent in the replication cycle of the fragmented replicases, and the loss of fragment diversity eventually halts self-replication.

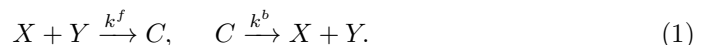
To find a way to resolve the above instability, we next examined the role of compartmentalization. Our model assumes a population of protocells (primitive cells; hereinafter referred to as “cells”), each encapsulating a finite number of fragments and replicases. We found that compartmentalization, in principle, allows the continued self-replication of the replicases by the stochastic correction mechanism [14, 15]. This mechanism is, however, severely limited in its applicability by its strict requirements on the number of fragments per cell and the population size of cells. Moreover, this mechanism is inefficient because it necessitates the continuous discarding of cells lacking some essential fragments and, therewith, a large number of fragments that could have produced functional replicases if combined across discarded cells.

Finally, we show that horizontal transfer between cells provides an efficient and

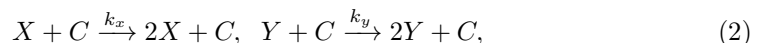
essential mechanism for the continued replication of the fragmented ribozymes. The previous studies on imperfect compartmentalization indicate that such horizontal transfer impedes the stochastic-correction mechanism [16, 17]. Therefore, horizontal transfer might be expected to be detrimental to the continued self-replication of the fragmented replicases. On the contrary, we found that the horizontal transfer of intermediate frequencies substantially stabilizes the system to such an extent that the parameter constraints imposed by the stochastic-correction mechanism are almost completely removed. This stabilization is caused by negative frequency-dependent selection, which arises through the interaction between the two distinct types of symmetry breaking, symmetry breaking between cells and symmetry breaking within cells, mediated by horizontal transfer.

## Model

We consider the simplest model of fragmented replicases, in which a catalyst consists of two fragments. The fragments (denoted by  $X$  and  $Y$ ) self-assemble into the catalyst (denoted by  $C$ ), and the catalyst disassembles into the fragments as follows:



We assume that the catalyst cannot replicate its own copies, but can replicate its fragments because shorter templates are more amenable to ribozyme-catalyzed replication as mentioned above. Therefore,



where the monomers are ignored under the assumption that their concentrations are buffered at constant levels, and complementary replication is ignored for simplicity. In the presence of the catalyst, each fragment replicates at a rate proportional to its copy number. Hence, the fragments undergo exponential amplification.

## Results

### Failure of balanced replication of fragments under a batch condition

First, we show that the replication of the fragments  $X$  and  $Y$  are unstable in a batch condition: replication is biased toward either of the fragments even if the rate constants for  $X$  and  $Y$  are identical, and the minor fragment is gradually diluted out from the system, so that the replication of the catalysts eventually stops. In this paper, we mainly focus on the situation where the rate constants are equal ( $k_x = k_y = k$ ) because our results remain qualitatively the same as long as the difference between  $k_x$  and  $k_y$  is sufficiently small.

We assume that the reactions undergo in a well-mixed batch condition so that the dynamics of the concentrations of  $X$ ,  $Y$ , and  $C$  (denoted by  $x$ ,  $y$ , and  $c$ , respectively) are written as follows:

$$\frac{dx}{dt} = (-k^f xy + k^b c + kxc) - x\phi \quad (3)$$

$$\frac{dy}{dt} = (-k^f yx + k^b c + kyc) - y\phi \quad (4)$$

$$\frac{dc}{dt} = (k^f xy - k^b c) - c\phi, \quad (5)$$

where  $\phi = k(x + y)c$ . In the right-hand side of these equations, the first terms in the brackets represent chemical reactions, and the second terms multiplied by  $\phi$  represent dilution. This dilution terms are introduced to fix the total concentration of fragments,  $x + y + 2c$ , since  $x$  and  $y$  increase through replication. Within the brackets enclosing the reaction terms, the first and second terms represent forward and backward reactions of 1, respectively. The third terms, which are present only in Equations 3 and 4, denote the replication of  $X$  and  $Y$  through reactions 2, respectively.

By introducing variables  $x_{tot} = x + c$  and  $y_{tot} = y + c$ , one can write

$$\frac{d}{dt} \begin{pmatrix} x_{tot} \\ y_{tot} \end{pmatrix} = \frac{kc^2}{y_{tot}^2} (x_{tot} - y_{tot}). \quad (6)$$

This equation indicates that a steady-state solution satisfies  $x_{tot} = y_{tot}$ . This solution is, however, unstable: a small increase in, say,  $x_{tot}$  over  $y_{tot}$  gets amplified because  $kc^2/y_{tot}^2$  is always positive, and, as a consequence, replication is biased to  $X$ . Intuitively, when  $x_{tot}$  is slightly greater than  $y_{tot}$ , the amount of free fragments  $x$  must also be greater than  $y$  because the same amount of  $X$  and  $Y$  are incorporated into catalysts. Therefore, the replication of  $X$  occurs more frequently than that of  $Y$  because more templates of  $X$  are available. As a result, the increase of  $x_{tot}$  is greater than that of  $y_{tot}$ . Because of this positive feedback, the concentration of the minor fragment  $Y$  gradually decreases as it is diluted out from the system, and, as a consequence, that of the catalysts  $C$  also decreases. Finally, the replication reaction stops once the catalysts are lost from the system.

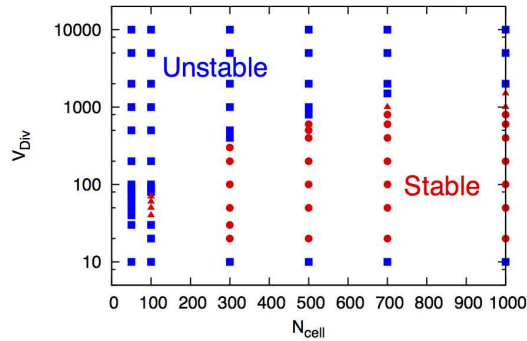
The instability of replication under a batch condition can be generally demonstrated for catalysts composed of an arbitrary number of fragments by straightforwardly extending the above model [see Supporting text section 1].

## Compartmentalization can overcome the unstable replication by selecting out non-growing cells but only under strong constraints on the sizes of cell volume and population

The introduction of compartments and their competitions can overcome the unstable replication. When the system is compartmentalized into a number of cells, stochasticity in cell compositions, competition for growth and division of cells provide a possible solution to avoid the loss of fragments: As the cells grow and eventually split into two with fragments distributed randomly between the daughter cells, cells with both  $X$  and  $Y$  fragments continue growth, while cells without either of them cannot grow. By introducing such a stochastic-correction mechanism at the cell level [14], one expects that the instability by the positive feedback at the molecule level can be resolved. To investigate this, we assume that the fragments and their assembly to function as a catalyst are partitioned into  $N_{cell}$  cells: the reactions occur in each cell. We adopted stochastic simulation using Gillespie algorithm [18] for reactions 1 and 2. We assume that the volume of each cell is proportional to the number of fragments inside, and as the number of fragments increases in a cell, the cell grows. When the total number of fragments reaches a threshold  $V_{Div}$ , the cell divides with the components randomly partitioned into two daughter cells. Here, at the division event, one randomly-chosen cell is removed to fix the total number of cells  $N_{cell}$ . By this cell-cell competition, cells with biased composition of  $X$  and  $Y$  are selected out because their growth is slow.

The relevant parameters for controlling the effect of compartmentalization are the division threshold  $V_{Div}$  and the number of cells  $N_{cell}$ . Figure 1A shows sets of the parameters with which the stochastic-correction mechanism can avoid the unstable replication, by suppressing the positive feedback and selecting cells keeping both

A Compartmentalization alone



B With horizontal transfer [ $D = 0.01$ ]

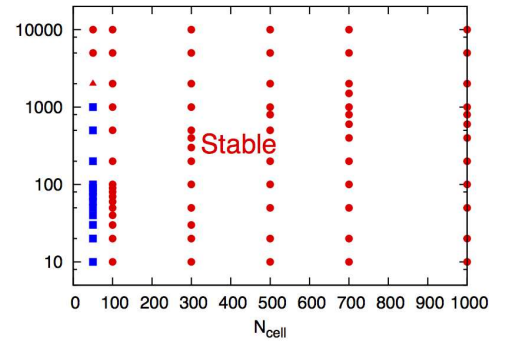


**Fig 1.** Sets of division threshold  $V_{Div}$  and the number of cells  $N_{cell}$  with which the unstable replication of reactions 1 and 2 are avoided by (A) compartmentalization alone and (B) that with horizontal transfer of the transfer constant  $D = 0.01$ . For the sets shown as stable [red circles], the system can continuously have cells with both fragments in the simulations up to  $4 \times 10^5$  division events from an initial condition where  $V_{Div}/4$  copies of each  $X$  and  $Y$  are in each cell. For the sets shown as unstable [blue squares], all cells with both fragments are lost from the system and it cannot continue growth. For the sets located at the boundary of stable and unstable area [shown in red triangles], the outcome depends on simulation runs.

fragments. If  $V_{Div}$  is very small (of the order of 10), the stochasticity of cell components is too strong to maintain both fragments continuously and either of them is lost for all cells. Hence, the system cannot continue growth. On the other hand, if  $V_{Div}$  is too large, stochasticity in components decreases. In each cell, the balance of fragments is broken, and the replication is biased to either of  $X$  or  $Y$ . Then, components of each cell are dominated by either of free  $X$  or  $Y$ , and the number of catalysts in dividing cells gradually decreases to one because at least one catalyst is necessary to replicate fragments. Even when the  $N_{cell}$  cells are separated into the equal number of  $X$ -dominant and  $Y$ -dominant cells, there is no frequency-dependent selection between the cells. Thus, the random drift will finally result in bias to either of  $X$ -dominant or  $Y$ -dominant cells. By division events, daughter cells without catalysts randomly replace remaining cells, therefore, the cells with catalysts are finally removed from the system.

For values of  $V_{Div}$  in-between, some of  $N_{cell}$  cells keep both  $X$  and  $Y$ , and can continue the replication. Besides  $V_{Div}$ , the number of cells  $N_{cell}$  is also restricted, to maintain such cells keeping both fragments  $X$  and  $Y$ . At division events, dividing cells without both fragments randomly replace remaining cells. Hence, when the number of cells  $N_{cell}$  is small, all the cells with both fragments will be finally removed. As the number of cells  $N_{cell}$  increases, the probability decreases that all the cells with both fragments are removed. As a result, the range of  $V_{Div}$  with stable replication increases. Note that the above cell-level selection mechanism is based on the removal of non-growing cells, and is inefficient because a large number of fragments in cells lacking some fragments must be continuously removed from the system although they are still functional if combined across the non-growing cells.

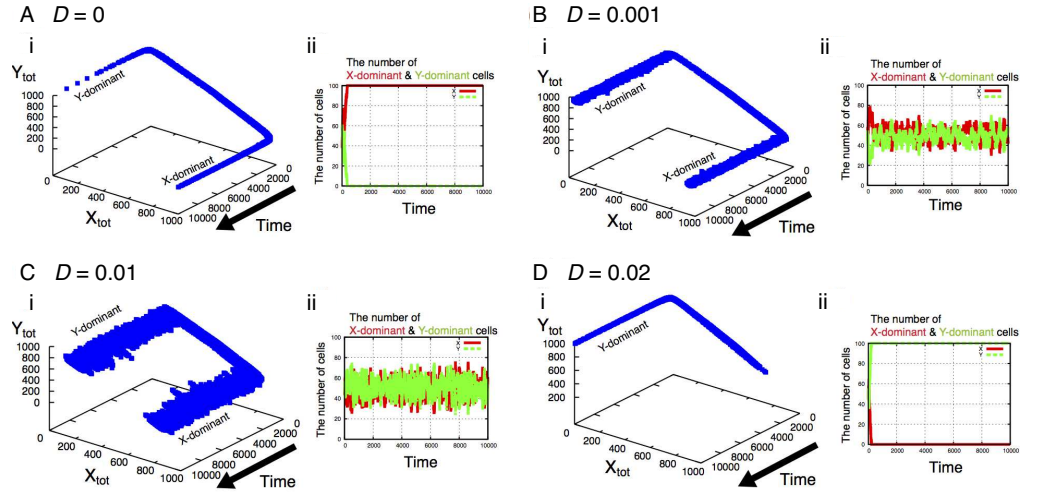


**Fig 2. (i) The number of fragments  $X_{tot}$  and  $Y_{tot}$  of dividing cells and (ii) the number of  $X$ -dominant and  $Y$ -dominant cells at corresponding time for the transfer rates (A)  $D = 0$  (B)  $D = 0.001$  (C)  $D = 0.01$  and (D)  $D = 0.02$ .**

Initially, the numbers of  $X_{tot}$  and  $Y_{tot}$  are approximately equal and, as time goes on, cells are differentiated into either of  $X$ -dominant or  $Y$ -dominant compositions. For  $D = 0$  (A), the system is unstable: only  $X$ -dominant cells (for this run) dominate (ii) and finally, cells cannot continue growth. For  $D = 0.001$  (B) and  $0.01$  (C), the system is stable;  $X$  and  $Y$  fragments coexist in each cell with unequal population (i). Here, the asymmetry between the major and minor fragments gets smaller as  $D$  increases. In addition, the two types of cells,  $X$ -dominant and  $Y$ -dominant cells coexist with the equal population (ii). As  $D$  increases further [ $D = 0.02$  (D)], the system gets unstable and only either of  $X$  or  $Y$  remains (ii). The parameters are  $V_{Div} = 1000$ ,  $N_{cell} = 100$ ,  $k^f = f^b = 1$ ,  $k_x = k_y = 1$ .

## Horizontal transfer of fragments with small rates removes the constraints of compartments for stable replication

Without the selection in cell population nor the restriction to  $V_{Div}$ , horizontal transfer of fragments between cells rescues the loss of fragments and enables continuous replication by maintaining the balance between  $X$  and  $Y$ . If the  $X$ -dominant and  $Y$ -dominant cells coexist in the cell population, the transfer between cells avoids loss of fragments for both cells by supplying fragments to each other because each fragment is in excess for cells on one side but lacking for cells on the other side.

For the purpose, we consider random mutual transfers of molecules among the  $N_{cell}$  cells. To implement the transfer, we consider reactions,  $X \xrightarrow{D} 0$ ,  $Y \xrightarrow{D} 0$ ,  $C \xrightarrow{D} 0$  so that the  $X$ ,  $Y$  and  $C$  are removed from a cell, respectively, with rate in proportional to each concentration, i.e.,  $Dx$ ,  $Dy$ , and  $Dc$ . This gives diffusion out of the cell. At the same time, the component is added to another randomly-chosen cell.

With the transfer among cells, the replication of the fragments is stabilized when the transfer constant  $D$  is small. In fact, the constraints of  $V_{Div}$  and  $N_{cell}$  are drastically eliminated [Figure 1B]. As long as the parameters are not extremely small, the stable replication continues. For small positive values of  $D$  [Figures 2B and C], the cell keeps on growing with the coexistence of  $X$  and  $Y$  molecules in each cell, even for large  $V_{Div}$  where only  $X$ -dominant or  $Y$ -dominant cells remain for  $D = 0$  [Figure 2A]. Here, the asymmetry between the fractions of the major and minor fragments gets

smaller as  $D$  increases. In addition, two types of cells,  $X$ -dominant and  $Y$ -dominant cells coexist roughly with equal population [Figures 2B(ii) and C(ii)]. As  $D$  is increased further [Figure 2D], the system gets unstable and only either of  $X$  or  $Y$  remains. This is natural, because for a large  $D$  limit, the system is well mixed, and the system is reduced back to the case without compartmentalization.

## Bifurcation explains the stable replication with small rates of horizontal transfer in two subsystems as an approximation of cell population

To answer why the small rates of transfer stabilizes the system, we approximate the dynamics of the population of cells by considering the dynamics of two subsystems between which the fragments are transferred. We assume the equal population of  $X$ -dominant and  $Y$ -dominant cells as two subsystems of equal volumes, namely, 1 and 2, respectively. We write the total concentration of  $X$  (the total of free  $X$ s and  $C$ s) of each subsystem as  $x_{tot}^1$  and  $x_{tot}^2$ , and the total of  $Y$  as  $y_{tot}^1$  and  $y_{tot}^2$ . The dynamics of  $x_{tot}^i$  in each subsystem ( $i = 1, 2$ ) is written as

$$\dot{x}_{tot}^1 = \frac{dx_{tot}^1}{dt} = F^1 - \frac{D}{2}x_{tot}^1 + \frac{D}{2}x_{tot}^2, \quad (7)$$

$$\dot{x}_{tot}^2 = \frac{dx_{tot}^2}{dt} = F^2 - \frac{D}{2}x_{tot}^2 + \frac{D}{2}x_{tot}^1. \quad (8)$$

where  $F^i = k(x_{tot}^i - c^i)c^i - x_{tot}^i\mu_i$ . The first term in  $F^i$  represents the replication of the component  $X$  by the first reaction of 2, where  $k$ ,  $(x_{tot}^i - c^i)$ , and  $c^i$  denote the rate constant, the concentrations of free  $X$  and  $C$  in subsystem  $i$ , respectively. The second term multiplied by  $\mu_i$  in  $F^i$  represents the dilution effect of the component due to the volume growth of the subsystem. The volume growth is assumed to keep the total concentration at unity (i.e.,  $x_{tot}^i + y_{tot}^i = 1$ ). Accordingly,  $\mu_i$  is defined as  $\mu_i = k(x_{tot}^i - c^i)c^i + k(y_{tot}^i - c^i)c^i = k(1 - 2c^i)c^i$ . Thus, in each subsystem, the components are diluted by the rate  $\mu_i$  in total. Then, the dilution rate of each component is proportional to the amount of the component, therefore, the component  $X_{tot}^i$  is diluted by the factor  $x_{tot}^i\mu_i$ . Along with the volume growth of each subsystem, we also assume that the total volume of both subsystems is fixed identical by removing components of each subsystem in proportion to its volume. This process corresponds to the random removal of cells to fix  $N_{cell}$  cells in our simulations, and the volume ratio of the subsystem 1 to 2 dynamically changes in general. In this section, we fix the two subsystems with an equal volume, whereas the dynamics of the volumes is investigated in the next section. Next, the second and third terms in Equations 7 and 8 denote average out- and in-flow of the components  $X$  by the transfer, respectively. These average flows are estimated as follows: the amount of the fragment  $X$  diffused out from the subsystem 1 is  $Dx_{tot}^1$ , but half of them is returned to the subsystem itself because, in our simulation, the population of cells is divided into  $X$ -dominant and  $Y$ -dominant cells with the equal population of  $N_{cell}/2$  and each fragment diffused out from a cell is randomly re-distributed into one of the cells, i.e., half of the fragments are distributed into  $X$ -dominant cells. Thus, the effective amount of fragments diffused out of subsystem 1 to 2 is  $Dx_{tot}^1/2$ . In the same manner, the effective amount of the fragment  $X$  for subsystem 1 received from subsystem 2 is approximated as halves of  $Dx_{tot}^2$ . The dynamics for  $Y$  are estimated in the same manner.

The fixed-point solutions of Equation 7 are analytically obtained by approximating  $c^i \approx 1 - \sqrt{1 - x_{tot}^i y_{tot}^i} \approx x_{tot}^i y_{tot}^i / 2$ . The first approximation assumes that the dynamics of reaction 1 is much faster than those of reactions 2 and transfers. The

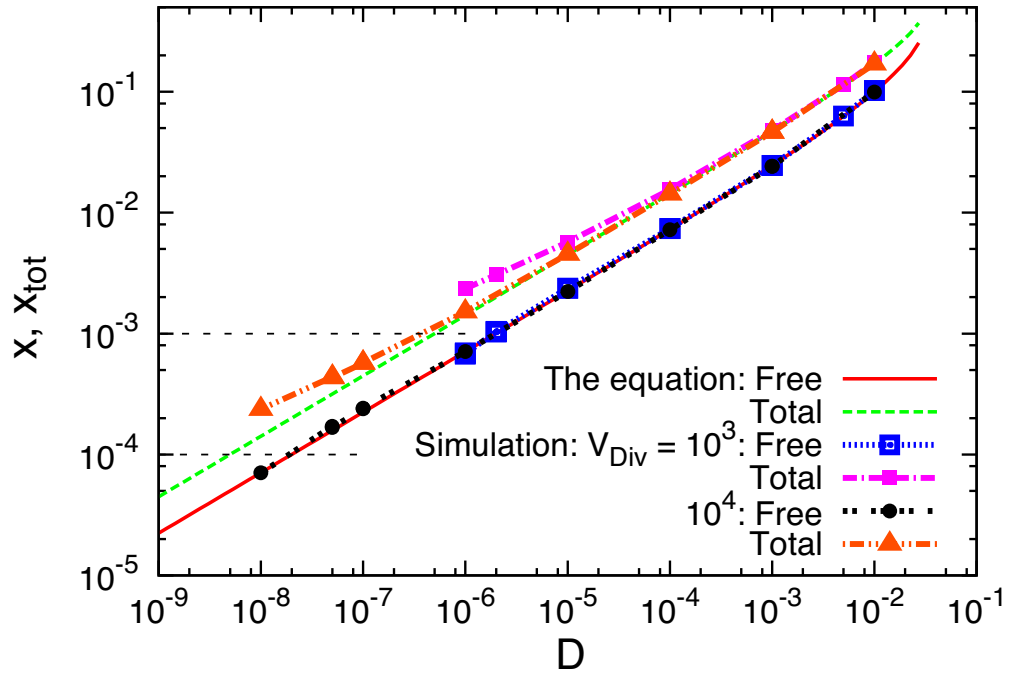


**Fig 3. The concentration  $x$  and  $x_{tot}$  at division events for  $Y$ -dominant cells as a function of  $D$ .** Free and Total indicate  $x$  and  $x_{tot}$ , respectively. For the free fragments [ $x$ ], the results of simulations [Blue and black curves for  $V_{Div} = 10^3$  and  $10^4$ ] agree well with the solution of Equation 10 [Red curve]. For the total fragments [ $x_{tot}$ ], the simulations [Magenta and orange curves for  $V_{Div} = 10^3$  and  $10^4$ ] agree with the solution of Equation 10 [Green curve] for larger  $D$ , but shift to larger values for smaller  $D$ . This is because cells must possess at least one catalyst to divide, therefore, the total fragments including  $c$  shift to larger values as it approaches the minimum requirement. For reference, the values of  $x_{tot} = 1/V_{Div}$  at which the number of  $c$  is equal to one for  $V_{Div} = 10^3$  and  $10^4$  are shown by horizontal dotted lines, respectively.



concentration of  $c^i$  is, then, approximated from the condition  $dc^i/dt = 0$  as  $c^i = 1 - \sqrt{1 - x_{tot}^i y_{tot}^i}$  for  $k^f = k^b$ . In addition, as we are interested in the stability of the system against the biased replication, we consider the case of highly-asymmetric composition, i.e.,  $x_{tot}^i y_{tot}^i \ll 1$ . Then, the second approximation  $c^i = x_{tot}^i y_{tot}^i / 2$  is obtained by using  $(1 - \epsilon)^{1/2} = 1 - \epsilon/2$  for  $|\epsilon| \ll 1$ . Using the approximations, the stable fixed point is obtained as

$$x_{tot}^1 = \frac{1}{2} \left( 1 + \sqrt{1 - 4\sqrt{2D/k}} \right), \quad (9)$$

and

$$x_{tot}^2 = \frac{1}{2} \left( 1 - \sqrt{1 - 4\sqrt{2D/k}} \right). \quad (10)$$

Here, we assume the dominant fragment of subsystem 1 is  $X$  and that of subsystem 2 is  $Y$  because  $x_{tot}^1 > 1/2$  and  $x_{tot}^2 < 1/2$ . Further, the relative value of the transfer rate  $D$  to the replication rate  $k$  is essential so that we fix  $k = 1$  below. The solution of the minor fragment  $x_{tot}^2$  is plotted as a function of the transfer rate  $D$  in Figure 3. As for the free fragments  $x^2 = x_{tot}^2 - c^2$ , it agrees well with the results of our simulation. For the total fragment  $x_{tot}^1$ , it agrees with the simulations for greater  $D$  although the results of simulation shift to larger values for smaller  $D$ , where the number of fragments decreases, but cells must possess at least one catalyst to divide, so that the total fragments including  $c$  shift to greater values as it approaches the minimum requirement, i.e., the total concentration of minor fragments be  $\geq 1/V_{Div}$ .

To study further the stability of the solution, we plot the flow [a direction of the vector  $(\dot{x}_{tot}^1, \dot{x}_{tot}^2)$ ] of Equation 7 in Figure 4. The steady-state solutions satisfy both  $\dot{x}_{tot}^1 = 0$  and  $\dot{x}_{tot}^2 = 0$ , therefore, they are represented as the crossing points of two nullclines [set of  $(x_{tot}^1, x_{tot}^2)$  satisfying  $\dot{x}_{tot}^1 = 0$  or  $\dot{x}_{tot}^2 = 0$ , indicated by blue and orange curves (see left-top panel)]. For  $D = 0$  [Figure 4A], a solution exists at  $(x_{tot}^1, x_{tot}^2) = (1/2, 1/2)$  (indicated by the light-blue square). However, it is unstable because the flows (arrows) point outward from the solution. Then, the system moves away from the solution by any tiny perturbation. The flows point toward each corner of the plane (indicated by the red triangles), where either of  $X$  or  $Y$  is lost and cells cannot grow. For small positive values of  $D$  [Figures 4B to D], stable fixed points (shown in red circles) appear to which the flows are directed from all directions, in addition to unstable fixed points (shown in blue squares) and the trivial solutions  $(x_{tot}^1, x_{tot}^2) = (0, 0), (1, 1)$  (shown in red triangles). Note that there exist two stable fixed points [red circles] for each  $D$  [Figures 4B to D], and the solution in Equation 9 corresponds to the right-bottom one.

As  $D$  increases, a bifurcation occurs at  $D = 0.02$  [Figure 4E] so that the stable fixed points for  $D \leq 0.02$  turn to be unstable (green stars). To understand this bifurcation, we consider eigenvectors  $v_1, v_2$  of Jacobian matrix of Equation 7 for the eigenvalues  $\lambda_1$  and  $\lambda_2$ . At the stable fixed points, they are obtained as  $v_1 = (1, 1)$  and  $v_2 = (1, -1)$  [see left-top panel in Figure 4]. The direction of  $v_1$  determines the asymmetry between  $X$  and  $Y$  in both subsystems. By moving along the  $v_1$ -direction of the plane, the amount of  $x_{tot}^1 + x_{tot}^2$  either increases or decreases while  $y_{tot}^1 + y_{tot}^2 = 2 - (x_{tot}^1 + x_{tot}^2)$  decreases or increases, respectively. On the other hand, the direction of  $v_2$  corresponds to the asymmetry between subsystems 1 and 2 for the fragments of  $X$ . By moving along the  $v_2$ -direction of the plane, the amount of  $x_{tot}^1$  increases or decreases while  $x_{tot}^2$  decreases or increases, respectively. The corresponding eigenvalues for  $v_1$  and  $v_2$  are calculated as  $\lambda_1 = 5D - \frac{\sqrt{2D}}{2}$  and  $\lambda_2 = 4D - \frac{\sqrt{2D}}{2}$ , respectively. As  $D$  increases, a bifurcation occurs first in  $v_1$ -direction at  $D^* = 0.02$  which is obtained from  $5D^* - \frac{\sqrt{2D^*}}{2} = 0$ . In fact, the flows (arrows) at the fixed point (green stars) are in the

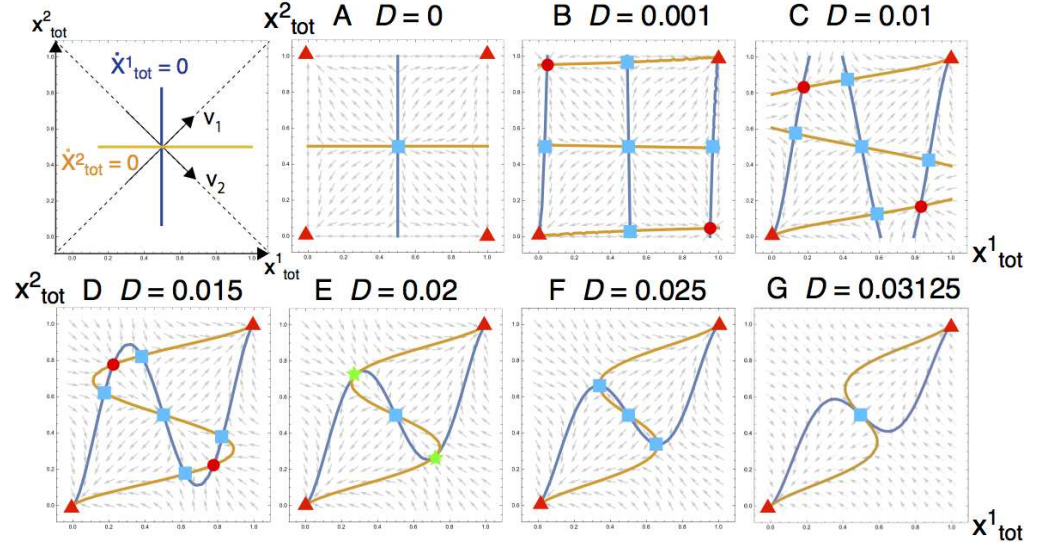


**Fig 4. Flow diagram of Equation 7.** As schematically indicated in the left-top panel, the nullclines are shown for  $\dot{x}_{tot}^1 = 0$  and  $\dot{x}_{tot}^2 = 0$  in blue and orange, respectively, and the crossing points of them are solutions. The directions of  $v_1 = (1, 1)$  and  $v_2 = (1, -1)$  are also indicated. For the solutions, stable fixed points are shown in red: those with stable growth [i.e., both fragments are in each subsystem] are in red circles, and those without growth [either of fragments is lost from subsystems or whole systems] are in red triangles. Unstable solutions are in light-blue squares, and neutral solutions in the  $v_1$ -direction are in green stars at  $D = 0.02$  (E). For  $D = 0$  (A), the solution exists at  $(x_{tot}^1, x_{tot}^2) = (1/2, 1/2)$  but it is unstable. For small values of  $D$  (B to D), the stable fixed points with growth [red circles] appear in addition to fixed points without growth. At  $D = 0.02$  (E), the fixed points with growth get unstable (shown in green stars) in  $v_1$ -directions. As  $D$  increases further (F), the two fixed points are still stable in  $v_2$ -directions, while the solution at  $(x_{tot}^1, x_{tot}^2) = (1/2, 1/2)$  is unstable in the direction. At  $D = 0.03125$  (G), the system transits from the three fixed points to one fixed point.

parallel direction of  $v_2$ , and point outward in the  $v_1$ -directions as  $D$  is increased further. This corresponds to the case in which the symmetry between  $X$  and  $Y$  breaks and only either of  $X$  and  $Y$  remains in both systems. The estimated value of  $D^*$  agrees with the results of our simulation [Figure 2]. In the two subsystems, the bifurcation also occurs in  $v_2$ -direction at  $D^+ = 0.03125$ , as obtained from  $4D^+ - \frac{\sqrt{2D^+}}{2} = 0$ , corresponding to the symmetry between subsystems 1 and 2. At the bifurcation point, the three fixed points (one unstable and two stable points in  $v_2$ -directions; shown all in light-blue squares) merge to one fixed point [Figure 4G].

The behavior of the bifurcations can be understood as follows. The system has two kinds of symmetry, one between fragments  $X$  and  $Y$ , and one between subsystems 1 and 2. For the stable replication, the symmetry between  $X$  and  $Y$  should be maintained because both fragments are essential. On the other hand, the symmetry between subsystems 1 and 2 should be broken because each fragment should be in excess for one subsystem, but lacking for the other subsystem. The two subsystems ‘help’ each other by the transfer of molecules. The former symmetry is maintained for  $0 \leq D < D^*$  and breaks for  $D > D^*$ . On the other hand, the latter symmetry is broken in the range  $0 \leq D < D^+$ . To meet the two conditions for the stable replication, the values of  $D$  are restricted as  $0 < D < D^* = 0.02$  because  $D^* < D^+$  ( $D = 0$  is eliminated by the condition each subsystem should contain both fragments).

### Frequency-dependent selection: why the balance of fragments is achieved at the cell population

In the previous section, we confirmed the stable replication by small rates of horizontal transfer, by assuming that the populations of two cell types are equal. Here, we verify that the state of the equal volume i.e. the equal population of  $X$ - and  $Y$ -dominant cells, is stable and selected as a result of a frequency-dependent selection. To analytically investigate the stability of the state, we consider the volume fractions of the subsystems 1 and 2 are slightly different from  $1/2$ , to be replaced by  $1/2 + \epsilon$  and  $1/2 - \epsilon$ , respectively, with  $\epsilon$  as a small parameter. Then the rate equations 7 and 8 are

$$\frac{dx_{tot}^1}{dt} = F^1 - D \left( \frac{1}{2} + \epsilon \right) x_{tot}^1 + D \left( \frac{1}{2} - \epsilon \right) x_{tot}^2, \quad (11)$$

$$\frac{dx_{tot}^2}{dt} = F^2 - D \left( \frac{1}{2} - \epsilon \right) x_{tot}^2 + D \left( \frac{1}{2} + \epsilon \right) x_{tot}^1, \quad (12)$$

where the replication and the dilution terms due to the volume growth are written as  $F^i = -x_{tot}^{i2}(1 - x_{tot}^i)^2(1 - 2x_{tot}^i)/4$  by substituting the approximation  $c^i = x_{tot}^i y_{tot}^i / 2$ .

Below, we show that the growth rate of the minor subsystem 2 with the fraction  $1/2 - \epsilon$  (for  $\epsilon > 0$ ) increases and the major subsystem 1 decreases, leading the fraction of the two subsystems to go back to equal. First, we write the concentrations of  $X$  at the steady state as  $x_{tot}^1 = x^* + \delta_1$  and  $x_{tot}^2 = 1 - x^* + \delta_2$  where  $x^* = \frac{1}{2} \left( 1 + \sqrt{1 - 4\sqrt{2D}} \right)$  is the solution for  $\epsilon = 0$  (Equation 9), and  $\delta_1$  and  $\delta_2$  are deviations caused by the introduction of  $\epsilon$ , respectively, for  $x_{tot}^1$  and  $x_{tot}^2$ . Then, from the steady state condition of Equations 11 and 12, one gets  $\delta_1 = \delta_2 = \frac{\sqrt{D}\epsilon}{\sqrt{2/2-4\sqrt{D}}}$ . The growth rates  $\mu_i$  ( $i = 1, 2$ ) are given by  $(x_{tot}^i - c^i)c^i + (y_{tot}^i - c^i)c^i$  so that

$$\mu_1 = \mu^* - \gamma(D)\epsilon, \quad (13)$$

$$\mu_2 = \mu^* + \gamma(D)\epsilon, \quad (14)$$

where  $\mu^* = \frac{\{1-x^*(1-x^*)\}x^*(1-x^*)}{2}$  is the growth rate at  $\epsilon = 0$ , and

$\gamma(D) = \frac{1-2\sqrt{2D}}{\sqrt{2}\sqrt{1-4\sqrt{2D}}}\sqrt{D} > 0$ , showing the decrease and the increase of the subsystem 1 and 2, respectively by  $\epsilon$ .

When  $\epsilon > 0$ , i.e., the volume of subsystem 1 exceeds that of 2, the concentrations of  $X$  in both subsystems 1 and 2 increase ( $\delta_1 = \delta_2 > 0$ ). For the subsystem 1, the fragment  $X$  is majority ( $x_{tot}^1 = x^* > 1/2$ ), therefore, the asymmetry between  $X$  and  $Y$  is enhanced by the increase of  $X$ . On the other hand, the fragment  $X$  is the minority in subsystem 2, and the composition of  $X$  and  $Y$  gets close to be symmetric by  $\delta_2$ . Because the growth rate is maximized when the concentrations of  $X$  and  $Y$  are equal, the rate  $\mu_1$  of subsystem 1 decreases, while that of 2,  $\mu_2$ , increases by the factor  $\gamma(D) > 0$  (see Equations 13 and 14). Consequently, the volume ratio of the two subsystems eventually goes back to equal. (Note that the frequency-dependent selection remains for any non-zero  $D$ , however, the replication is unstable in our simulation for small values of  $D$  when discreteness in molecule number is taken into account [see Supporting text section 2]).

## Discussions

In summary, we have shown that the self-replication of fragmented replicases is unstable under a simple batch condition. Replication is biased towards a subset of the fragments and eventually stops due to the lack of an essential fragment. Although the stochastic-correction mechanism induced by compartmentalization helps, it imposes severe restrictions on the number of molecules per cell and the population size of cells. In addition, the mechanism is inefficient because a large number of fragments in non-growing cells must be discarded. Finally, we have shown that the horizontal transfer of intermediate frequencies provides an efficient and favorable solution to the instability of the fragmented replicases.

Recent experimental studies have been challenged to use self-assembling fragmented ribozymes to synthesize each of the component fragments to achieve the RNA-catalyzed exponential amplification of the ribozyme itself [9]. The self-assembly of functional RNA polymerase ribozymes from short RNA oligomers has been demonstrated by driving entropically disfavored reactions under iterated freeze-thaw cycles [7]. Our theoretical results predict that these approaches for (re-)constructing RNA-based evolving systems have the serious issue: the replication of fragments is inevitably biased, so that it eventually fails to produce the copies of the ribozymes. Simultaneously, our study proposes a solution for this issue: the random exchange of fragments between loose compartments at intermediate frequencies.

Recent experiments suggest that the random exchange of contents between compartments is plausible. The freeze-thaw cycles, which enhance the assembly of fragments [7], also induce content exchange between giant unilamellar vesicles through diffusion [19] or through fusion and fission [20]. Also, transient compartmentalization, which involves the occasional complete mixing of contents between compartments, is considered to be relevant to maintain functional replicators [17, 21–24]. Taken together, it therefore seems natural to assume that compartmentalization is imperfect enough to allow the random exchange of fragments between compartments at the primitive stages of life.

The model of fragmented replicases investigated above can be conceptually compared to the hypercycle [25], a model proposed to solve error catastrophes: Both models posit that multiple distinct sequences are integrated into an auto-catalytic system, which as a whole maintains a greater amount of information than possible by a single sequence. However, the two models sharply differ in dynamical aspects. In the fragmented replicases, the dynamics involves the positive feedback, which biases

replication toward a subset of the fragments. In the hypercycle, the dynamics involves negative feedback, which balances the replication of distinct sequences on a long timescale, but also causes oscillatory instability on a short timescale. Given these comparisons, horizontal transfer as studied here will be also relevant to hypercycles. In addition, hypercycles entail evolutionary instability due to parasites [26]. It would be interesting to study the effect of parasites on the fragmented ribozymes in the future.

## Supporting information

**Supporting text. Supporting information with sections on 1) General extension of the replication to  $N$ -fragments ribozymes; 2) Unstable growth for small transfer rate in our simulation of compartments is due to discreteness of molecules in cells.**

## Acknowledgments

This research is partially supported by a Grant-in-Aid for Scientific Research(S) (15H05746) from the Japan Society for the Promotion of Science(JSPS).

## References

1. Joyce GF. The antiquity of RNA-based evolution. *Nature*. 2002;418(6894):214.
2. Higgs PG, Lehman N. The RNA World: molecular cooperation at the origins of life. *Nature Reviews Genetics*. 2015;16(1):7.
3. Johnston WK, Unrau PJ, Lawrence MS, Glasner ME, Bartel DP. RNA-catalyzed RNA polymerization: accurate and general RNA-templated primer extension. *Science (New York, NY)*. 2001;292(5520):1319–25. doi:10.1126/science.1060786.
4. Zaher HS, Unrau PJ. Selection of an improved RNA polymerase ribozyme with superior extension and fidelity. *RNA (New York, NY)*. 2007;13(7):1017–26. doi:10.1261/rna.548807.
5. Wochner A, Attwater J, Coulson A, Holliger P. Ribozyme-catalyzed transcription of an active ribozyme. *Science (New York, NY)*. 2011;332(6026):209–12. doi:10.1126/science.1200752.
6. Attwater J, Wochner A, Holliger P. In-ice evolution of RNA polymerase ribozyme activity. *Nature Chemistry*. 2013;5(12):1011–1018. doi:10.1038/nchem.1781.
7. Mutschler H, Wochner A, Holliger P. Freeze–thaw cycles as drivers of complex ribozyme assembly. *Nature chemistry*. 2015;7(6):502.
8. Horning DP, Joyce GF. Amplification of RNA by an RNA polymerase ribozyme. *Proceedings of the National Academy of Sciences of the United States of America*. 2016;113(35):9786–91. doi:10.1073/pnas.1610103113.
9. Horning DP, Samantha B, Tjhung KF, Joyce GF. RNA-Catalyzed Polymerization and Replication of RNA. In: XVIIIth International Conference on the Origin of Life. vol. 1967 of LPI Contributions; 2017. p. 4067.

10. Attwater J, Raguram A, Morgunov AS, Gianni E, Holliger P. Ribozyme-catalysed RNA synthesis using triplet building blocks. *eLife*. 2018;7:e35255. doi:10.7554/eLife.35255.
11. Segré D, Ben-Eli D, Lancet D. Compositional genomes: prebiotic information transfer in mutually catalytic noncovalent assemblies. *Proceedings of the National Academy of Sciences*. 2000;97(8):4112–4117.
12. Furusawa C, Kaneko K. Zipf’s law in gene expression. *Physical review letters*. 2003;90(8):088102.
13. Kamimura A, Kaneko K. Exponential growth for self-reproduction in a catalytic reaction network: relevance of a minority molecular species and crowdedness. *New Journal of Physics*. 2018;20(3):035001.
14. Szathmáry E, Demeter L. Group selection of early replicators and the origin of life. *Journal of theoretical biology*. 1987;128(4):463–486.
15. Szathmáry E, Smith JM. The major evolutionary transitions. *Nature*. 1995;374(6519):227–232.
16. Fontanari JF, Serva M. Effect of migration in a diffusion model for template coexistence in protocells. *Bulletin of Mathematical Biology*. 2014;76(3):654–672. doi:10.1007/s11538-014-9937-7.
17. Blokhuis A, Lacoste D, Nghe P, Peliti L. Selection Dynamics in Transient Compartmentalization. *Phys Rev Lett*. 2018;120:158101. doi:10.1103/PhysRevLett.120.158101.
18. Gillespie DT. Exact stochastic simulation of coupled chemical reactions. *The Journal of Physical Chemistry*. 1977;81(25):2340–2361. doi:10.1021/j100540a008.
19. Litschel T, Ganzinger KA, Movinkel T, Heymann M, Robinson T, Mutschler H, et al. Freeze-thaw cycles induce content exchange between cell-sized lipid vesicles. *New Journal of Physics*. 2018;20(5):055008.
20. Tsuji G, Fujii S, Sunami T, Yomo T. Sustainable proliferation of liposomes compatible with inner RNA replication. *Proceedings of the National Academy of Sciences*. 2016;113(3):590–595. doi:10.1073/pnas.1516893113.
21. Matsuura T, Yamaguchi M, Ko-Mitamura EP, Shima Y, Urabe I, Yomo T. Importance of compartment formation for a self-encoding system. *Proceedings of the National Academy of Sciences*. 2002;99(11):7514–7517.
22. Ichihashi N, Usui K, Kazuta Y, Sunami T, Matsuura T, Yomo T. Darwinian evolution in a translation-coupled RNA replication system within a cell-like compartment. *Nature communications*. 2013;4:2494.
23. Bansho Y, Furubayashi T, Ichihashi N, Yomo T. Host–parasite oscillation dynamics and evolution in a compartmentalized RNA replication system. *Proceedings of the National Academy of Sciences*. 2016;113(15):4045–4050.
24. Matsumura S, Kun Á, Ryckelynck M, Coldren F, Szilágyi A, Jossinet F, et al. Transient compartmentalization of RNA replicators prevents extinction due to parasites. *Science*. 2016;354(6317):1293–1296.
25. Eigen M, Schuster P. *The Hypercycle: A Principle of Natural Self Organization*. Berlin: Springer-Verlag; 1979.
26. Smith JM. Hypercycles and the origin of life. *Nature*. 1979;280:445–446.

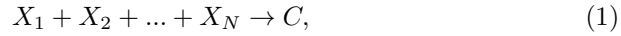
# Supplementary Information for Horizontal transfer between loose compartments stabilizes replication of fragmented ribozymes

Atsushi Kamimura, Yoshiya J. Matsubara, Kunihiro Kaneko, Nobuto Takeuchi

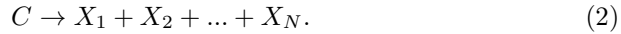
January 2019

## 1 General extension of the replication to $N$ -fragments ribozymes

One could straightforwardly extend the two-fragments to general  $N$ -fragments system, in which  $N$  fragments of  $X^i$  ( $i = 1, \dots, N$ ) assemble to form the catalyst. The assembly of the catalyst from the  $N$ -fragments is written as



and the catalyst disassemble into the  $N$ -fragments as



Each of the fragments replicates with the aid of the catalyst  $C$  as



for  $i = 1, \dots, N$ .

The dynamics of the fragments  $X_i$  and the catalyst  $C$  are written as

$$\frac{dx^i}{dt} = (-x^1 x^2 \dots x^N + c) + x^i c - x^i \phi, \quad (4)$$

and

$$\frac{dc}{dt} = (x^1 x^2 \dots x^N - c) - c\phi, \quad (5)$$

where  $x^i$  and  $c$  denote the concentrations of  $X_i$  and  $C$ , respectively. Here, all the rate constants are fixed to one. In the right-hand-side of the equations, the terms in the brackets denote the assembly (1) and the disassembly (2) of the catalyst, and the second term in Equation (4) denotes the replication of the fragment  $X^i$  (3). Each of the last terms with  $\phi$  represents dilution. The dilution

terms with  $\phi = (1 - Nc)c$  are introduced to fix total number of fragments as  $\sum_i (x^i + c) = \sum_i x^i + Nc = 1$ .

By adding both ends of Equations (4) and (5), one can write the dynamics of total concentration of  $X^i$  (total of free  $X^i$  and that in the catalyst),  $x_{tot}^i$  ( $i = 1, \dots, N$ ) as

$$\frac{dx_{tot}^i}{dt} = (x_{tot}^i - c)c - x_{tot}^i \phi,$$

where the concentration of the free  $X_i$ ,  $x^i$ , is written as  $x_{tot}^i - c$ . Then, for arbitrary pair of  $i$  and  $j$  ( $i, j = 1, \dots, N$ ), one obtains

$$\frac{d}{dt} \left( \frac{x_{tot}^i}{x_{tot}^j} \right) = \frac{c^2}{x_{tot}^{j2}} (x_{tot}^i - x_{tot}^j) \quad (6)$$

Given that  $(c/x_{tot}^j)^2$  is positive, this indicates that a small increase of  $x_{tot}^i$  over  $x_{tot}^j$  grows so that the solution is unstable of balanced replication  $x_{tot}^i = x_{tot}^j$  for every pair of  $i$  and  $j$ .

## 2 Unstable growth for small transfer rate in our simulation of compartments is due to discreteness of molecules in cells

The bifurcation analysis presented in the main text explains that the system is stable for infinitely small but non-zero values of  $D$  for the two subsystems. On the other hand, the system gets unstable in our simulation of compartments for small non-zero values of  $D$ , because the system is dominated by either of the  $X$ - or  $Y$ -dominant cells and the symmetry between  $X$  and  $Y$  is broken.

As  $D$  decreases, the system is dominated by either of the cells because fluctuations increase between the number of  $X$ - and  $Y$ -dominant cells and, once the number of either type of cells reaches the population size  $N_{cell}$ , it irreversibly breaks the symmetry between  $X$  and  $Y$ . Actually, the variances  $\sigma^2$  of the number of  $X$ -dominant cells increases as  $D$  decreases [Fig. S1A].

The increase of the variances suggests that pressure of the frequency-dependent selection to maintain the symmetry is getting weak as  $D$  decreases. However, the analysis up to the first order of  $\epsilon$  presented in the main text does not explain such dependence on  $D$  for the two subsystems. The pressure to maintain the symmetry is represented by relative values of the factor  $\gamma(D)$  to the average growth rate  $\mu^*$  in Equations 13 and 14 of the main text. If the relative values decrease with decreasing  $D$ , the pressure would be weakened because the relative increase or decrease of the growth rates, respectively, between subsystems of smaller or larger volumes gets smaller. Actually the factor  $\gamma(D)$  depends on  $D$  as  $\sqrt{D}$  for small  $D$  [see Fig. S2], but the average growth rate  $\mu^*$  also scales as  $\sqrt{D}$ . Therefore, the relative pressure of the frequency-dependent selection does not change with decreasing  $D$ .



This suggests that the unstable growth in our simulation of compartments is due to the discrete nature of molecules in cells because the effect is neglected in the two subsystems. As  $D$  decreases, the number of minor fragments decreases [Fig. 3 of the main text], therefore, the cells gradually contain only a few or no catalyst. In fact, the number of cells with the catalysts  $C$  gradually decreases with decreasing  $D$  [Fig. S1B: the case for both  $X/Y$ -fragments and catalysts also shows similar curves] in accordance with the increase of the variances  $\sigma^2$  of the number of  $X$ -dominant cells [Fig. S1A]. Therefore, the discrete nature of molecules in cells contributes to the enhancement of variations between cells and consequently results in the increase of the variances.

A scaling behavior between the transfer rate  $D$  and the division threshold  $V_{Div}$  is also consistent with the enhancement of the variances by the discreteness of molecules. The relevant values of the transfer rate  $D$  with which the effect of the discrete number of molecules appears scales as  $1/V_{Div}^2$ . For substantially small  $D$ , the concentration of minor fragments in Equation 10 of the main text can be written as  $x_{tot}^1 = \sqrt{2D}$ . Therefore, the values of  $D$  at which the total number of minor fragments is approximately equal to one scale as  $D \approx 1/2V_{Div}^2$ . In fact, the numbers of cells with  $X$  fragments and catalysts  $C$  and the variances for different  $V_{Div}$  and  $N_{cell}$  agree as one plot as a function of  $DV_{Div}^2$  [Fig. S1C and D]. This suggests that, when  $V_{Div}$  is infinitely large, the variances do not increase even when  $D$  decreases to infinitely small.

Further, the system is stable if the number of cells  $N_{cell}$  is large because the variances of the ratio of  $X$ -dominant to  $Y$ -dominant cells scales as  $1/\sqrt{N_{cell}}$  with  $N_{cell}$ . The variances  $\sigma^2$  of the number of  $X$ -dominant cells divided by  $N_{cell}$  collapses into the same curves for different  $N_{cell}$  [Fig. S1D]. This indicates that they increase with  $\sqrt{N_{cell}}$ , and the ratio of  $X$ -dominant cells to total population scales as  $1/\sqrt{N_{cell}}$ . Thus, fluctuations in the ratio of  $X$ -dominant to  $Y$ -dominant cells decrease when  $N_{cell}$  is getting large.

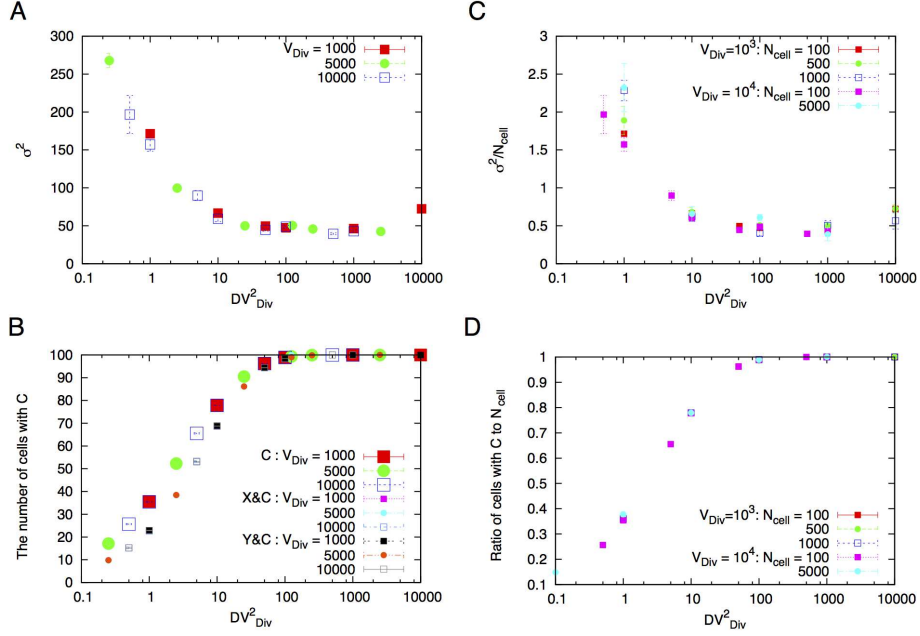


Figure S1: (A) Variances  $\sigma^2$  of the number of  $X$ -dominant cells as functions of  $D$  and  $V_{Div}$ . Here,  $N_{cell} = 100$ . (B) The number of cells with catalysts  $C$  scales with  $DV_{Div}^2$  for  $V_{Div} = 1000, 5000, 10000$ . The numbers of cells with both  $C$  and free  $X/Y$  also show a similar curve. Here,  $N_{cell} = 100$ . (C) Variances  $\sigma^2$  of the number of  $X$ -dominant cells divided by  $N_{cell}$  and (D) Ratio of cells with the catalysts  $C$  to  $N_{cell}$  are shown for different values of  $N_{cell}$ . All the points follow the same curve under the scaling  $DV_{Div}^2$ .

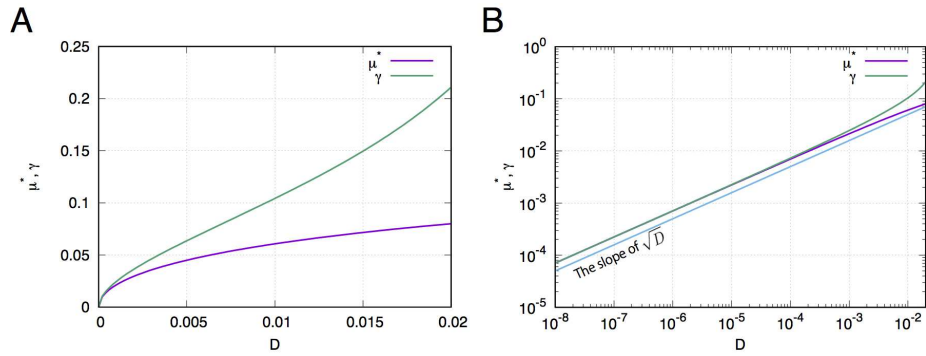


Figure S2: Growth rate  $\mu^*$  and  $\gamma(D)$  of Equation 13 and 14 of the main text as a function of  $D$  in (A) normal and (B) log-log scale for small  $D$ . The slope  $\sqrt{D}$  is also shown in (B).